CMS Endcap RPC Performance Analysis*

H. Teng（滕海云）[1;1)], Y. Ban（班勇）[1;2)]，J. Cai（蔡建新）[1]，Z. Xue（薛志华）[1]，
Y. Ge（葛榆成）[1]，S. Qian（钱思进）[1]，Y. Mao（冒亚军）[1]，Y. Ye（叶沿林）[1]，
S. Costantini [2], K. Beernaert [2], A. Cimmino [2], G. Garcia [2], J. Lellouch [2],
A. Marinov [2], A. Ocampo [2], N. Strobbe [2], F. Thyssen [2], M. Tytgat [2],
P. Verwilligen [2], E. Yazgan [2], N. Zaganidis [2], A. Dimitrov [3], R. Hadjiiska [3],
L. Litov [3], B. Pavlov [3], P. Petkov [3], A. Aleksandrov [4], V. Genchev [4],
P. Iaydjiev [4], M. Rodozov [4], M. Shopova [4], G. Sultanov [4], C. Avila [5],
L.F. Chaparro [5], J.P. Gomez [5], B. Gomez Moreno [5], A.F. Osorio Oliveros [5],
J.C. Sanabria [5], Y. Assran [6], A. Sharma [7], M. Abbrescia [8], C. Calabria [8],
A. Colaleo [8], F. Loddo [8], M. Maggi [8], G. Pugliese [8], L. Benussi [9],
S. Bianco [9], S. Colafranceschi [9], D. Piccolo [9], S. Buontempo [10], C. Carrillo [10],
O. Iorio [10], P. Paolucci [10], U. Berzano [11], M. Gabusi [11], P. Vitulo [11],
M. Kang [12], K.S. Lee [12], S.K. Park [12], S. Shin [12], Y. Choi [13],
J. Goh [13], M.S. Kim [13], H. Seo [13] and M. Shoaib [14]

[1] School of Physics, State Key Laboratory of Nuclear Physics and Technology, Peking University, Beijing 100871, China
[2] University of Ghent, Department of Physics and Astronomy, Proeftuinstraat 86, B-9000, Ghent, Belgium
[3] University of Sofia, Faculty of Physics, Atomic Physics Department, 5, James Bourchier Boulevard, BG-1164 Sofia, Bulgaria
[4] Bulgarian Academy of Sciences, Inst. for Nucl. Res. and Nucl. Energy, Tzarigradsko shaussee Boulevard 72, BG-1784 Sofia, Bulgaria
[5] Universidad de Los Andes, Apartado Aereo 4976, Carrera 1E, no. 18A 10, CO-Bogota, Colombia
[6] Academy of Scientific Research and Technology of the Arab Republic of Egypt, 101 Sharia Kasr El-Ain, Cairo, Egypt
[7] Panjab University, Department of Physics, Chandigarh Mandir 160 014, India
[8] Universita e INFN, Sezione di Bari, Via Orabona 4, IT-70126 Bari, Italy
[9] INFN, Laboratori Nazionali di Frascati (LNF), PO Box 13, Via Enrico Fermi 40, IT-00044 Frascati, Italy
[10] Universita e INFN, Sezione di Napoli, Complesso Univ. Monte S. Angelo, Via Cintia, IT-80126 Napoli, Italy
[11] Universita e INFN, Sezione di Pavia, Via Bassi 6, IT-Pavia, Italy
[12] Korea University, Physics Department, Seoul Cheongryangri 143-701, Republic of Korea
[13] Sungkyunkwan University, Department of Physics, 2066, Seobu-ro, Jangan-gu, Suwon, Gyeonggi-do, Republic of Korea
[14] National Centre for Physics, Quaid-E-Azam University Islamabd, Pakistan

Abstract:

The Resistive Plate Chamber (RPC) detector system in LHC-CMS experiment is designed for trigger and timing purpose. The endcap RPC system has been successfully operated since the construction and installation up to 2008. Although the chambers have been tested extensively during the construction phase, a thorough check using collision data is necessary to understand the detector performance. We developed an efficiency analysis tool and analyzed the collision data, focusing on the first endcap station which was assembled and tested by Peking University. We obtained the reliable detector efficiency performance, and helped to decide the RPC working high voltage level during data taking. We also tried to analyze other RPC performance characteristics such as spatial resolution. The results showed that, the CMS-RPC endcap system has satisfactory performance as expected during data taking in LHC collision experiment.

Key words: RPC, detector efficiency, CMS experiment

PACS: 29.40.Cs

Received 00 March 2014

∗ Supported by National Natural Science Foundation of China (11061140514)

1) E-mail: hyteng@pku.edu.cn

2) E-mail: bany@pku.edu.cn

1 Introduction

The Compact Muon Solenoid (CMS) [1] is one of the general purpose experiments at Large Hadron Collider (LHC)experiment [2], the physics motivation is to test the Standard Model and to explore the new physics, especially to search for the Higgs boson. The CMS detector consists of various sub-detector systems [1]. Among them, the muon system located outside of the magnetic coil was designed for trigger purpose, as well as for measuring the track of muons which could easily penetrate the calorimeter and iron absorber. The muon system used three technologies: the Drift Tube (DT) and Resistive Plate Chamber (RPC) in barrel region, and the Cathode Strip Chamber (CSC) and also RPC in endcap region.

The RPC detector system was designed for trigger and timing purpose, while CSC and DT also provide muon tracking measurement. For triggering performance, a 95% efficiency for RPC is required. Each chamber was tested extensively using cosmic rays after the assembly, the results agreed well with the expectation, showing high efficiency (96%) and good time and space behavior [3–8]. Since year 2008 the endcap RPC system has been installed on CMS yokes and started commissioning.

During the initial online operation, several algorithms were applied to evaluate the detector efficiency. This study tries to validate one of the efficiency calculation algorithm, which takes neighboring CSC segment signal as trigger.

The CMS muon system layout in endcap region is described in Section 2, especially the RPC system topology, which is the base for RPC performance analysis. The principle of the efficiency analysis algorithm is explained in Section 3. In Section 4 we used MC simulation to examine our algorithm, with detailed survey on seemingly low efficiency behavior and possible bias discrimination. The endcap RPC performance with collision data using the updated tool is illustrated in Section 5.

2 Endcap RPC System

According to the position along the beam pipe, which is also the z axis in CMS global coordination, the two symmetric muon endcaps were indexed as plus and minus endcap, each endcap is further divided into four disks with three supporting iron yokes between them. Each disk composed of two kinds of muon detectors (CSC and RPC) to form a station, which makes up individual layers along particle trajectory in track reconstruction. The three iron yokes which also serve as absorber are labeled as YE1/YE2/YE3.

The CSC system is settled on 4 stations, until 2012 the fourth station was only partly installed. Station 2, 3 and 4 contain two circular rings of chambers at different radius, the outer ring (labeled as ring2) is divided into 36 segments in azimuth ϕ, each segment covers 10 degrees with one CSC chamber; while the inner ring (ring1) is divided into 18 segments, thus each chamber covers 20 degrees. Station 1 has three rings and are all divided into 36 segments. On all rings the first segment starts approximately at $\phi = -5°$, and the index grows with increasing ϕ. The mounting scheme of CSC and RPC will also affect the trigger calculation in efficiency analysis. The CSC chambers in four stations were mounted on different surfaces of the iron yokes [9].

The endcap RPC system has similar layout, the chambers are installed in the first three stations by 2008, labeled as RE1/RE2/RE3, while RE4 station is scheduled to be installed in 2013-2014 LHC shut-down period. Each RPC station is further divided into three rings along the radius. At present only the two low η rings (ring2 and ring3) were fully installed, the high η region (ring1, near the beam-pipe) is staged for future plan. In RE1 station, the RPC ring were mounted adjacent to the corresponding CSC ring. In RE2 and RE3 stations, RPC ring 2 plus ring 3 cover the same area as CSC ring 2. The readout strips inside each RPC chamber in ring 2 and ring 3 of all stations were divided into three sections (roll a, b, c) along the radius. The endcap RPC detector layout is shown in Fig. 1 [10]. In the following text, we' ll use the index of station/ring/roll to label RPC position, for example, RE+1/3/b refers to RPC section in +z endcap station 1, ring 3 and roll b.

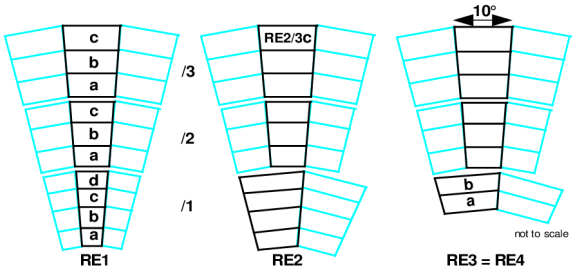

Fig. 1. The scheme of the endcap RPC system. The signal division (rolls) in different rings is shown for each station. The ϕ coverage of the detectors on each ring keeps the same as the adjacent CSC detectors.

The CMS RPC detector has a double Bakelite gas-gaps structure, as shown in Fig. 2 [11]. The signal readout strips were put between the gas-gaps. The inner surfaces of the gas-gaps were treated with the linseed oil to suppress the noises. An electrical field will be setup by the high voltage applied to the graphite surfaces, the energy deposited by the particles passing through the gas-gaps will cause ionization, leads to an avalanche or streamer process depending on the strength of electrical

field and the gas composition, then the signal induced on strips will be readout.

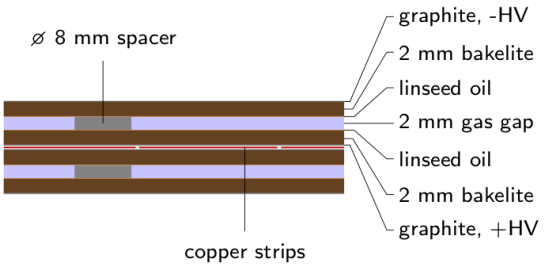

Fig. 2. The structure of the RPC detector. The double gas-gaps and the sandwich readout strip scheme will provide high efficiency.

CMS-RPC operates in avalanche mode [10]. The avalanche production depends on the environmental pressure P, the temperature T, the gas mixture and the high voltage HV. At fixed gas-mixture, the dependence parameter could be summarized as an effective high voltage [11–14] in Eq. (1):

$$HV_{eff} = HV\frac{P_0}{P}\frac{T}{T_0}, \tag{1}$$

where $P_0 = 965mbar$, $T_0 = 293K$. The dependence on HV is described by a sigmoidal shape as in Eq. (2), where $HV_{50\%}$ is the effective high voltage when the chamber reaches the half of its maximum efficiency ε_{max}, S is a parameter indicating the steepness of the sigmoid [11, 15]:

$$\varepsilon = \frac{\varepsilon_{max}}{1+e^{-S\left(HV_{eff}-HV_{50\%}\right)}}, \tag{2}$$

RPC detector use a digital readout, the spatial resolution is related to the mean strip width and the cluster size (the average number of fired strips per signal) [16]:

$$RMS_{expected} = \frac{<strip \quad width> \times <cluster \quad size>}{\sqrt{12}}, \tag{3}$$

The CMS endcap RPC project was shared by institutes in Italy, Korea, Pakistan, Belgium, China and CERN. Peking University is responsible for the production of detector structure materials, and the assembly and test of RE1 ring2 and ring3 chambers [5–7, 17–19].

3 Efficiency Analysis Algorithm

The online RPC efficiency is calculated using CSC signal as trigger. Each CSC chamber is adjacent to one or two RPC chambers, its track segment will be straightly extrapolated to the adjacent RPC surface, to serve as a trigger to test RPC efficiency, as shown in Fig. 3. An acceptance window is applied to compare the residual distance between the impact position and the cluster center of the fired strips. In the analysis this threshold is fixed to the width of 4 strips (the strip width of the endcap RPC is about 2 cm). Event was marked as efficient if the residual is within the threshold, or the fired cluster center is found inside the acceptance window.

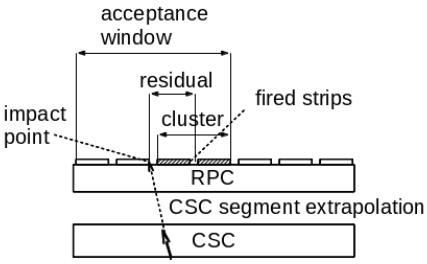

Fig. 3. CSC track segment extrapolation: the impact position is evaluated by extrapolate a single CSC track segment straightly to the corresponding RPC detector surface. Residual between the fire position and the impact position is measured, and an acceptance windows is applied to determine the efficiency.

The RPC efficiency is evaluated as the counting rate ratio between the acknowledge RPC events and CSC triggered events. Eq. (4) and Eq. (5) specify the estimation of efficiency and its error:

$$\varepsilon_{RPC} = \frac{N_{RPC}}{N_{CSC}} \tag{4}$$

$$\Delta\varepsilon = \sqrt{\frac{\varepsilon_{RPC}\times(1-\varepsilon_{RPC})}{N_{CSC}}}. \tag{5}$$

Two solutions are introduced to suppress the fake trigger events. First, a filter of CSC segments is specified by the trajectory characteristics. Assume the global direction of the sampled segment and another segment from the adjacent station are (θ_1,ϕ_1) and (θ_2,ϕ_2), respectively, the direction variance ΔR is defined as

$$\Delta R = \sqrt{(\theta_1-\theta_2)^2+(\phi_1-\phi_2)^2}. \tag{6}$$

ΔR will be used as the parameter of "segment match filter" to estimate the trigger segment. Segments from the trajectory should take coincident direction, and the value of ΔR should be below the threshold, while trigger from noise will not be able to take a pattern segment on chambers in next station, thus could not pass the filter.

The second measure is to remove the fake trigger on the edges of RPC roll, which is caused by the inaccuracy of CSC measurement and the segment extrapolation. Here the uncertainties in CSC measurement and segment extrapolation are expressed by corresponding tolerance range in θ and ϕ, which produces a pyramidal projection onto RPC surface, while actually the impact tolerance on RPC surface could be identified with a cone projection. Only the events with cones fully inside the RPC sensitive area will be counted, those with part of cone projection outside the RPC roll are skipped as fake trigger events. On the other hand, the adjacent RPC rolls are overlapped each other at side edges on most rings, if the cone covers two adjacent RPC rolls, both of them will become candidate to find the possible acknowledgement.

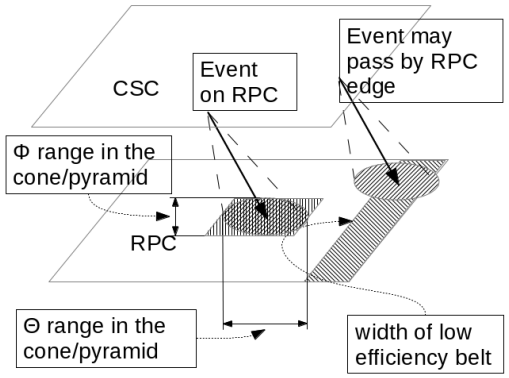

Fig. 4. The definition of CSC track segment cone in extrapolation used to estimate measurement bias. The cone projection indicates if the actual trajectory could possibly pass by the edge of RPC surface.

The cone algorithm was validated with the MC simulation. A $\Delta R = 0.2$ segment match threshold was applied to filter out CSC noise events, while the filter is cancelled in RE1/3/b and RE1/3/c due to empty match on segment match filter, which is caused by the special CSC geometry layouts there. Then with a $-0.2rad$ cone size along θ direction, the fake trigger events on top/bottom edge of the RPC roll were cut out. Meanwhile, a very small cone size (0.01 in radian) along ϕ direction was set to check the overlapping region on the side edges of RPC chamber, in case of the segment extrapolation hit there. The result is shown in Fig. 5. We see that the expected efficiency performance was achieved using the CSC segment extrapolation trigger, a 95% of efficiency is represent on all RPC surface, thus the software tool is verified to be reliable from MC simulation, and is ready to be used in real data.

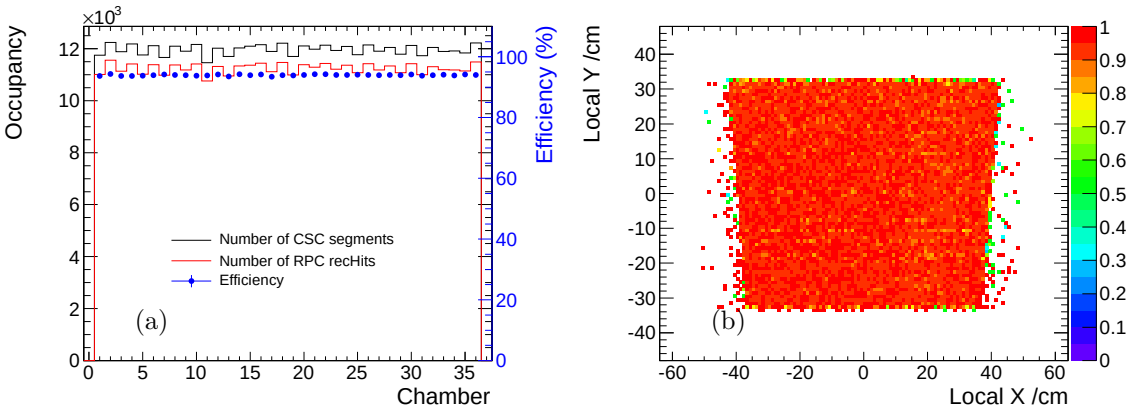

Fig. 5. (color online) RPC efficiency distribution from MC simulation, the CSC segment cone criteria was applied. The analysis of RE+1/3/b MC data is shown here as an example: (a) RPC efficiency and the occupancies of both RPC and CSC versus chamber number of all 36 chambers in the ring, (b) the merged 2D efficiency distributions on RPC surface.

4 Endcap RPC Performance from 2010 Data

The was analyzed With the reliable software tool, we analyzed the endcap RPC performance using 2010 collision data. The RPC performance studies focused on barrel RPC was reported in Ref. [14, 16, 20]. During the 2010 LHC collision period, the endcap RPC system was operated under 3 different HV settings: $9400V$, $9500V$ and $9550V$, the thresholds of frond end electronics were set to $220mV$. The dark current, which was strongly affected by variations of environmental conditions such as

temperature and humidity, turned out to be stable during the commission except in some case of HV ramping. Generally the average value was less than $3uA$ [21], some chambers with too high dark current or other HV/LV off problems were masked, a black list corresponding to run number was applied to filter out those rolls during performance analysis. The same parameters optimized in MC study were set during online performance analysis, i.e., $\Delta R = 0.2$ except for RE1/3/a and RE1/3/b, cone angle width in θ was $-0.2rad$, in ϕ was $0.01rad$.

4.1 Efficiency

The results of 2010 collision data analysis shows that, most RPC rolls have an efficiency over 95% at higher operation HV. Some low efficiency rolls mainly worked under single gap mode, with HV only applied on one gas gap in the chamber, thus reduced the efficiency. Fig. 6 shows the efficiency in run 147755 with HV at $9500V$, all the rolls work at an efficiency around 95%.

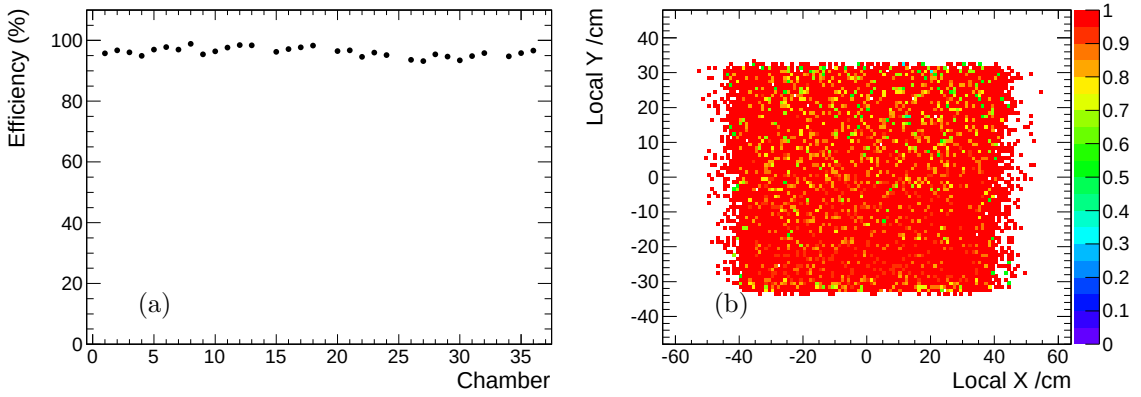

Fig. 6. (color online) RPC efficiency distribution from collision data (run 147755, luminosity is $0.5153pb^{-1}$, HV was set at $9500V$). The RE+1/R3 roll b data is shown here as an example: (a) efficiency versus chamber number of all 36 chambers in the ring, the masked chambers are removed from calculation. Low efficiency chambers mostly worked in single gap mode; (b) merged 2D efficiency distributions on RPC surface.

Presently installed CMS endcap RPC system has totally 432 chambers, each chamber is divided into 3 rolls in η direction. The efficiency distribution on all individual rolls is surveyed in Fig. 7 from all 2010 data at $HV = 9500V$.

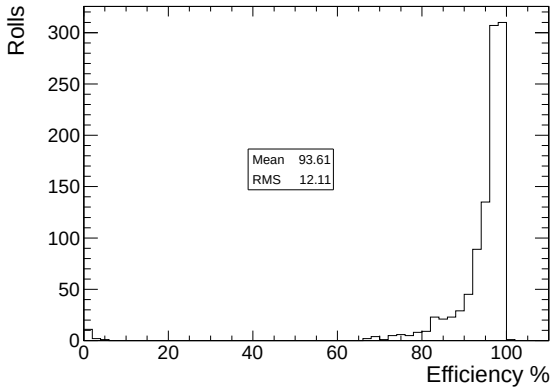

Fig. 7. Efficiency distribute on all RPC rolls from 2010 data at $HV = 9500V$.

Fig. 8 shows the 2D efficiency distributions over the RE+1/R2/a surface, where all data at $HV = 9500V$ were merged together to assure enough statistics. We see clearly the regularly distributed low efficiency spots on the surface, which correspond to the spacers inside the gas gap structure. These distributions confirm that the software tool works correctly and could well survey the efficiency homogeneity on RPC chamber surface.

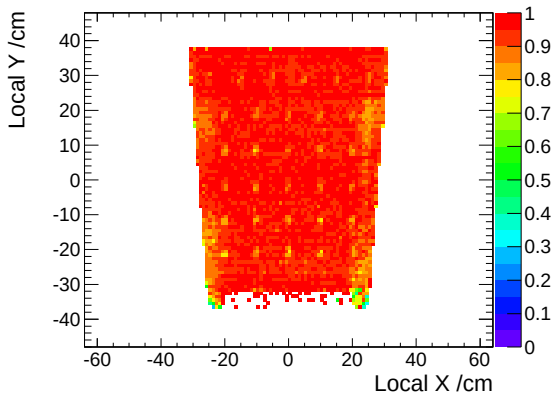

Fig. 8. (color online) Merged 2D efficiency distributions over the RE+1/2/a surfaces, for all 2010 data at $HV = 9500V$. The regularly distributed low efficiency spots correspond to the spacers inside the gas gap structure.

By checking the efficiency fluctuation with the temperature and pressure variation at the same time period(Fig. 9), we found that they are correlated and follow similar trend.

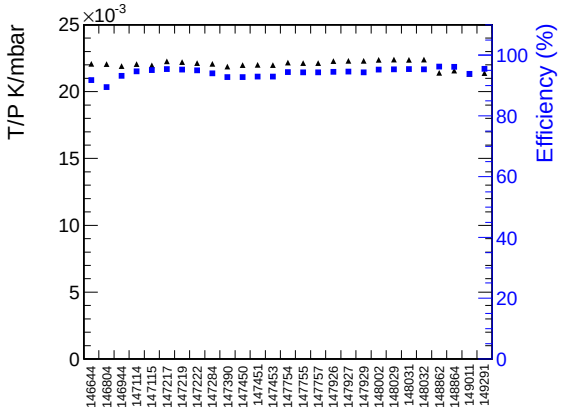

Fig. 9. (color online) Average RPC efficiency with respect to the run numbers. The efficiency fluctuation is correlated to the temperature and pressure variation.

4.2 Spatial Resolution

The spatial resolution is also crucial for endcap RPC system to provide a reliable trigger, and to further complete the function of muon track reconstruction. It is surveyed by cluster size and residual distribution.

Cluster size is the number of average fired strips per signal, it is relevant to the trigger generation, which use the RPC hit pattern to determine trajectory parameters such as transverse momentum and charge. Fig. 10 shows the cluster size distribution from collision data at $HV = 9500V$. Most events have cluster size not larger than 3. The large cluster size events are related to the hit position on strips, deposited energy and the incident angle of the muons trajectories, in which case two or more independent avalanches were produced in double gas-gaps and induced signals on multi strips. The correlation between incident angle and cluster size is surveyed as shown in Fig. 11. Fig. 12 shows the fluctuation of average cluster size with respect to the run number (or environmental parameters), similar behavior as in efficiency case was observed, which implies the effective HV have similar influence on cluster size.

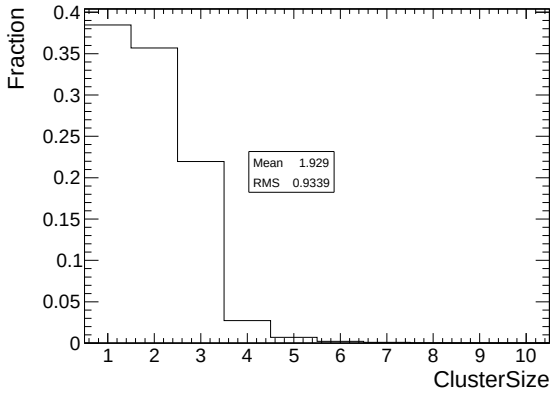

Fig. 10. The distribution of cluster size at $HV = 9500V$ runs.

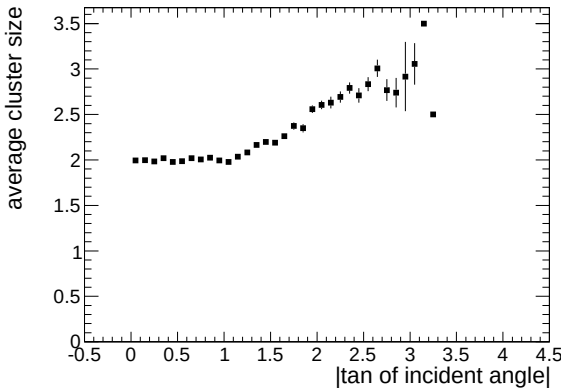

Fig. 11. Correlation between the average cluster size and the incident angle on RE+1/3/b. The error corresponds to the RMS of the cluster size within each bin.

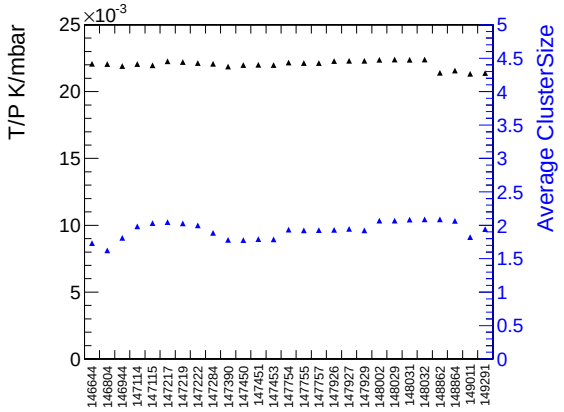

Fig. 12. (color online) The average cluster size with respect to run number or environmental parameters, showing the correlation with the pressure and temperature fluctuation. The error corresponds to the RMS of the cluster size.

Fig. 13 shows the residual distribution at $HV = 9500V$, which is defined as the distance between the RPC

fired strip and the impact position extrapolated from CSC muon track. For RE+1/2 the width at the middle of the trapezoidal strip is 2.093cm, the average cluster size is measured to be 2.253, so the expected spatial resolution is calculated to be 1.361 (Eq. (3)). From the residual distribution, we measured the RMS to be 1.161. The difference between the calculated resolution and measurement might come from that, the endcap strip is trapezoidal and the impact position is not evenly distributed on the strip surface.

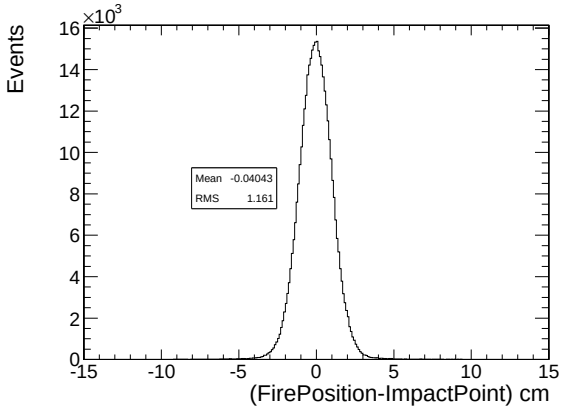

Fig. 13. Residual distributions: the distance between the RPC fired strip and the impact position extrapolated from CSC muon track, on RE+1/2/b.

5 Summary

Considering the geometry layout of CMS endcap muon system, we developed an appropriate software tool to measure the RPC efficiency using extrapolated CSC track segment as trigger. We checked and validated the efficiency algorithm by MC simulation, the software tool resumed the performance of endcap RPC to the expected level from MC study. With the validated tool we surveyed the endcap RPC performance in 2010 collision data; The result shows that, the RPC operated well as expected under appropriate HV setting. With such good performance in efficiency and spatial resolution, as well as its excellent timing, the endcap RPC could provide stable and reliable trigger function for physics program. From 2011 and 2012 data similar conclusion could be derived.

The authors are grateful to all colleagues of CMS RPC and CSC communities for the helpful discussions and suggestions. This work is financed by National Natural Science Foundation of China under project No.11061140514.

References

1 The CMS Collaboration. The CMS experiment at CERN LHC. JINST, Augest 2008, 3, S08004
2 L.Evans, P.Bryant. LHC Machine. JINST, Augest 2008, 3, S08001
3 M. Abbrescia et al. Production and test of one-third of barrel Resistive Plate Chambers of the CMS experiment at LHC. Nucl.Instrum.Meth.A, December 2004, 535(1-2): 283-286
4 M. Abbrescia et al. The cosmic rays quality test procedure for the CMS barrel resistive plate chambers. Nucl.Instrum.Meth.A, November 2004, 533(1-2): 208-213
5 Z. Aftab et al. Assembly and Quality Certification for the First Station of CMS Endcap RPCs (RE1). Nucl.Phys.B.Proc.Suppl, Augest 2006, 158: 103-107
6 Z. Aftab et al. Production and the quality control for the CMS endcap RPCs. Nucl.Phys.B.Proc.Suppl, Augest 2006, 158: 16-20
7 A.Ball et al. Cosmic Ray Test Certification of the First 100 CMS Endcap RPCs and the Corresponding Construction Database. Nuclear Physics B (Proc.Suppl.), Augest 2006, 158: 99-102
8 M. Abbrescia et al. Production and quality control of the Barrel RPC chambers of the CMS experiment. Nucl.Phys.B.Proc.Suppl, January 2006, 150: 290-294
9 R. Breedon, T. Cox, W. Ko et al. CSC Strip, Wire, Chamber, and Electronics Conventions. CMS IN 2007/024
10 The CMS Collaboration. The CMS muon project : Technical Design Report. 1997
11 Filip Thyssen. Performance of the Resistive Plate Chambers in the CMS experiment. JINST, January 2012, 7, C01104
12 Lippmann et al. Detector Physics of Resistive Plate Chambers. CERN-THESIS-2003-035
13 Werner Riegler, Christian Lippmann, Rob Veenhof. Detector physics and simulation of resistive plate chambers. Nucl.Instrum.Meth.A, March 2003, 500(1-3): 144-162
14 CMS Collaboration. Performance study of the CMS barrel resistive plate chambers with cosmic rays. JINST, March 2010, 5, T03017
15 M. Abbrescia et al. Cosmic ray tests of double-gap resistive plate chambers for the CMS experiment. Nucl.Instrum.Meth.A, September 2005, 550(1-2): 116-126
16 Camilo Carrillo. The CMS RPC project, results from 2009 cosmic-ray data. Nucl.Instrum.Meth.A, January 2012, 661: S19-S22
17 Ying J, Ye YL, Ban Y et al. Study of an avalanche-mode resistive plate chamber. J.Phys.G, Augest 2000, 26(8): 1291-1298
18 Ying J, Ye YL, Ban Y et al. Beam test results of a resistive plate chamber made of Chinese Bakelites. Nucl.Instrum.Meth.A, March 2001, 459(3): 513-522
19 Ye YL, YING J, BAN Y et.al. Study of Resistive Plate Chambers for muon detection at LHC. 中国科学, 2002, 32(4):299
20 D. Piccolo et al. Resistive Plate Chambers performance with Cosmic Rays in the CMS experiment. Nucl.Instrum.Meth.A, May 2010, 617(1-3): 180-182
21 CMS Collaboration. CMS Online Web Based Monitoring. CMS internal website.